Unconventional superconductivity near a flat band in organic and organometallic materials

Jaime Merino [ORCID],[1] Manuel Fernández López [ORCID],[1] and Ben J. Powell[2]

[1]*Departamento de Física Teórica de la Materia Condensada, Condensed Matter Physics Center (IFIMAC) and Instituto Nicolás Cabrera, Universidad Autónoma de Madrid, Madrid 28049, Spain*

[2]*School of Mathematics and Physics, The University of Queensland, QLD 4072, Australia*

We study electron correlation driven superconductivity on a decorated honeycomb lattice (DHL), which has a low-energy flat band. On doping, we find singlet superconductivity with extended-s, extended-d, and f-wave symmetry mediated by magnetic exchange. f-wave singlet pairing is enabled by the lattice decoration. The critical temperature is predicted to be significantly higher than on similar lattices lacking flat bands. We discuss how high-temperature superconductivity could be realized in the DHL materials such as $Rb_3TT \cdot 2H_2O$ and $Mo_3S_7(dmit)_3$.

I. INTRODUCTION

The recent discovery of superconductivity in twisted bilayer graphene has lead to intense theoretical investigations of Cooper pairing in nearly flat band systems. The observation of superconductivity close to correlated insulating states in twisted bilayer graphene [1–3] suggests that Coulomb repulsion plays a major role in its electronic properties including, possibly, superconductivity. Flat bands enhance Coulomb scattering—since scattering processes with any transferred momenta are allowed within the flat band—leading to novel pairing states [4]. Prior to the discovery of superconductivity in twisted bilayer graphene [5], flat band systems were proposed as a route towards room temperature superconductivity [6,7] due to linear scaling of the critical temperature with the coupling. These considerations are very general and motivate the search for superconducting materials, beyond twisted bilayer graphene, with flat bands [8].

Electrons on the decorated honeycomb lattice [DHL; Fig. 1(a)] can display many interesting properties including topological phases [9–14]. The DHL has a flat band at the Fermi energy when half filled and lightly hole doped [$0 \leqslant \delta < 1/3$, where the number of electrons per site is $n = 1 - \delta$; Fig. 2 (inset)]. This leads to a large density of states so one expects strong electronic correlation effects close to half filling [15]. The DHL is realized in several materials including trinuclear organometallic compounds [16–20], organic molecular crystals [21], iron(III) acetates [22], coordination polymers/metal-organic frameworks (MOFs) [23,24], and cold fermionic atoms in optical lattices [25]. An important open question is whether superconductivity from Coulomb interaction can arise in DHL compounds as theoretically predicted in graphene [26,27] and in the closely related lattice arising in Li-decorated graphene [28], LiC_6.

Numerical work [13,29,30] indicates that the ground state of the spin-1/2 Heisenberg model on a DHL with nearest-neighbor interactions is a valence bond solid (VBS). Two different VBSs are suggested depending on the anisotropy [J'/J; Fig. 1(a)]. Subtle changes in the lattice and interactions can radically change this—indicating that there are many competing ground states. For example, the ground state of the Kitaev model on the DHL is a quantum spin liquid (QSL) [31]. A QSL is also predicted for the Heisenberg model on the kagomé lattice [32–35], which is closely related to the DHL. In contrast, longer range interactions and/or higher order spin exchange are needed to stabilize a QSL on the (anisotropic) triangular lattice [36–39].

Anderson's resonating valence bond (RVB) hypothesis [40] is that unconventional superconductivity can arise when one dopes holes into a Mott insulator as valence bonds become mobile (singlet) Cooper pairs. Therefore, if VBSs occur at half filling on the DHL [13,29,30], then an important issue is to understand the conducting phases that arise upon hole doping. Similar programs have been carried out in the context of the (square lattice) cuprate superconductors [40,41] and the (anisotropic triangular lattice) organic superconductors [42,43]. Due to the greater complexity of the DHL we can expect, in general, pairing states other than the d and $d + id$ states generally found on the square and anisotropic triangular lattices [41–44]. Similar conclusions have been recently reached in strongly correlated multiorbital inorganic materials [45].

Here, we report on the existence of unconventional superconductivity, including an f-wave singlet state [Fig. 1(e)], in the hole doped DHL arising from Coulomb repulsion. Successive transitions from extended-s (s^*) to extended-d (d^*) to f-wave superconductivity occur at low temperatures (Fig. 2). The highest critical temperature in our phase diagram occurs around (7–8)% doping where s^* superconductivity is most favorable. The superconducting critical and pseudogap temperatures are much larger than the corresponding ones on the square [46] and triangular lattices [42,43,47,48]. Hence, the robustness of the superconducting and pseudogap phases is correlated with the flat band at the Fermi energy in the DHL.
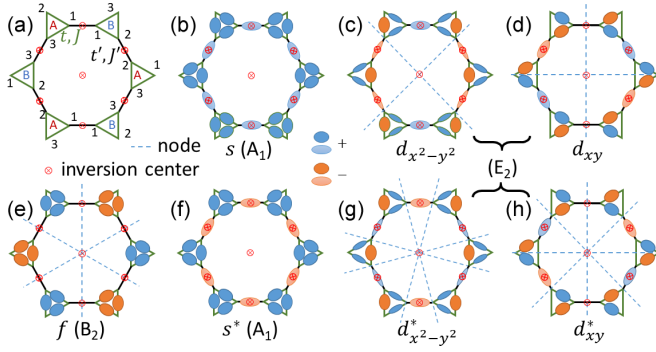
094517-1

FIG. 1. Decorated honeycomb lattice and its superconducting phases. (a) The decorated honeycomb lattice with the hopping (t, t') and exchange (J, J') parameters marked. The triangles form two sublattices (A and B) and contain three sites (labeled 1–3). (b)–(h) Real space representations of selected singlet superconducting states on the decorated honeycomb lattice. Color (size) of the ovals indicates the sign (magnitude) of the order parameter (Δ, Δ'). The decorated lattice allows an f-wave spin singlet state and extended-s and -d (s^* and d^*) states which are consistent with the 2D irreducible representation of C_{6v} (Table I). The states in the bottom row (e)–(h) are found in our microscopic calculations.

II. f-WAVE SINGLET PAIRING

At first glance, an f-wave singlet state seems to violate the requirement that the wave function must be antisymmetric under the exchange of two fermions (electrons). Usually one thinks that if the wave function is odd under spatial inversion ($\mathbf{k} \rightarrow -\mathbf{k}$) then it must be even under spin inversion ($\sigma \rightarrow -\sigma$); thus, the f-wave state must be a spin triplet. But, this
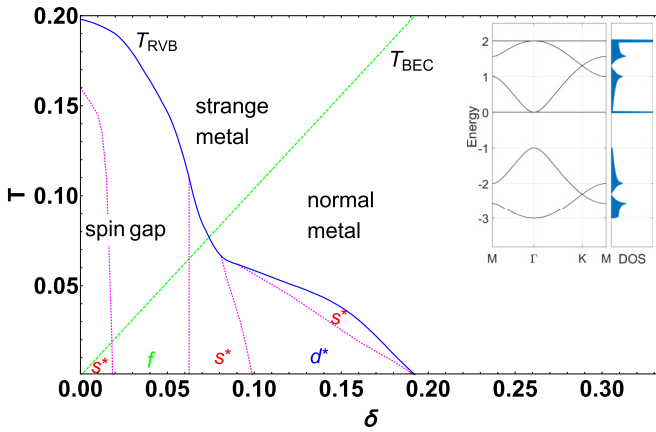

FIG. 2. Phase diagram of the t-t'-J-J' model on a decorated honeycomb lattice for $J/t = 0.1$ and $t'/t = J'/J = 1$. Pairing in unconventional channels s^*, d^*, and f occurs below the mean-field pairing temperature (T_{RVB}; blue solid line). Charge transport is coherent below the Bose-Einstein condensation temperature, T_{BEC}. Superconductivity requires both pairing and coherence, i.e., $T < T_{RVB}$ and T_{BEC}. The dotted (magenta) lines are first order transitions between different superconducting states while the solid (blue) line corresponds to a second order transition between superconducting and metallic states. Inset: The noninteracting band structure of the decorated honeycomb lattice displaying flat bands and the corresponding DOS for $t' = t$. $t = 1$ in all plots.

argument does not account for the internal degrees of freedom within the unit cell of the DHL—which can be described as either the site labels or as molecular orbital degrees of freedom [16].

Insight into f-wave singlet states can be gained from writing a (nonsuperconducting) two-electron wave function, $|\Psi_-\rangle$, that is odd under both spatial and spin inversion for a single unit cell of the DHL. Let $|\Psi_\alpha\rangle = (h^\dagger_{\alpha 1, \alpha 2} + h^\dagger_{\alpha 2, \alpha 3} + h^\dagger_{\alpha 3, \alpha 1})|0\rangle$, where the singlet operator $h^\dagger_{\alpha i, \beta j} = \frac{1}{\sqrt{2}}(c^\dagger_{\alpha i \uparrow} c^\dagger_{\beta j \downarrow} - c^\dagger_{\alpha i \downarrow} c^\dagger_{\beta j \uparrow})$ and $c^\dagger_{\alpha i \sigma}$ creates an electron with spin σ on the ith site of the αth triangle. Define $|\Psi_\pm\rangle \equiv |\Psi_A\rangle \pm |\Psi_B\rangle$: Both wave functions are a superposition of singlets within the triangles (and therefore singlets themselves) and satisfy fermionic antisymmetry for any pair of electrons, but whereas $|\Psi_+\rangle$ is even under inversion, $|\Psi_-\rangle$ is odd [49]. The f-wave singlet superconducting state in Fig. 1 is highly analogous to $|\Psi_-\rangle$.

III. MODEL

Our microscopic theory considers the t-t'-J-J' model on the DHL:

$$
\begin{aligned}
H = &-t \sum_{\langle \alpha i, \alpha j \rangle \sigma} P_G(c^\dagger_{\alpha i \sigma} c_{\alpha j \sigma} + c^\dagger_{\alpha j \sigma} c_{\alpha i \sigma}) P_G \\
&-t' \sum_{\langle Ai, Bi \rangle, \sigma} P_G(c^\dagger_{Ai\sigma} c_{Bi\sigma} + c^\dagger_{Bi\sigma} c_{Ai\sigma}) P_G \\
&-J \sum_{\langle \alpha i, \alpha j \rangle} \left(\mathbf{S}_{\alpha i} \cdot \mathbf{S}_{\alpha j} - \frac{1}{4} n_{\alpha i} n_{\alpha j} \right) \\
&-J' \sum_{\langle Ai, Bi \rangle} \left(\mathbf{S}_{Ai} \cdot \mathbf{S}_{Bi} - \frac{1}{4} n_{Ai} n_{Bi} \right) - \mu \sum_{\alpha i \sigma} c^\dagger_{\alpha i \sigma} c_{\alpha i \sigma},
\end{aligned}
$$

$$(1)$$

where $\mathbf{S}_{\alpha i} = \sum_{\sigma \sigma'} c^\dagger_{\alpha i \sigma} \boldsymbol{\tau}_{\sigma \sigma} c_{\alpha i \sigma'}$, $\boldsymbol{\tau}$ is the vector of Pauli matrices, $n_{\alpha i} = \sum_\sigma c^\dagger_{\alpha i \sigma} c_{\alpha i \sigma}$, and the Gutzwiller projector $P_G = \Pi_i (1 - n_{i\uparrow} n_{i\downarrow})$ excludes doubly occupied sites. The sums are restricted to nearest-neighbor sites either within a triangle, $\langle \alpha i, \alpha j \rangle$, or between neighboring triangles, $\langle Ai, Bi \rangle$, cf. Fig. 1(a). The chemical potential μ fixes the average electron filling of the system. Motivated by the superexchange mechanism, and to reduce the number of free parameters, we set $J'/J = (t'/t)^2$ in all of our calculations. We solve this model via RVB theory [41,50], where double occupancy is projected out of a Bardeen-Cooper-Schrieffer (BCS) wave function via the Gutzwiller approximation (GWA). Technical details including an exact analysis of pairing symmetries on small clusters [51] are given in Ref. [49].

IV. SUPERCONDUCTIVITY

The DHL has C_{6v} symmetry, which has six irreducible representations (Table I), three even and three odd under inversion symmetry [in 2D, inversion is equivalent to a C_2 rotation about the 'z axis': both map $(x, y) \rightarrow (-x, -y)$]. The order parameters most relevant to our RVB calculations are sketched in Fig. 1. This includes a B_2 ($f_{x(3y^2-x^2)}$, henceforth f-wave) state built from a superposition of singlets. This state

TABLE I. Character table for C_{6v}. The n-fold rotations (C_n) are about the center of the dodecahedron, σ_d reflections are defined to pass through the center of t' bonds, and σ_v are reflections through the line joining a vertex and the center of a triangle, cf. Fig. 1. The last column gives the conventional name of the superconducting symmetry.

	E	$2C_6$	$2C_3$	C_2	$3\sigma_v$	$3\sigma_d$	Superconducting order
A_1	1	1	1	1	1	1	s, s^*
A_2	1	1	1	1	-1	-1	$i_{xy(3x^4-10x^2y^2+3y^4)}$
B_1	1	-1	1	-1	1	-1	$f_{y(3x^2-y^2)}$
B_2	1	-1	1	-1	-1	1	$f_{x(3y^2-x^2)}$
E_1	2	1	-1	-2	0	0	(p_x, p_y)
E_2	2	-1	-1	2	0	0	$(d_{x^2-y^2}, d_{xy}), (d^*_{x^2-y^2}, d^*_{xy})$

is odd under inversion through the center of the dodecahedron ($\cong C_2$) and under inversion through the center of the t' bonds (equivalent to a σ_v mirror), but it is even under the σ_d mirrors (which bisect the triangles). This is consistent with fermionic exchange statistics because the singlets are all within a single triangle that decorate the honeycomb lattice—the nodes lie on the intertriangle bonds along the σ_v mirror planes. p-wave singlets are also possible on this lattice via a similar construction (with nodes along the t' bonds) [52]. However, the p-wave states are not low-energy solutions in our singlet RVB states.

Odd-parity f- and p-wave singlet states are not allowed on the honeycomb lattice because the triangles are replaced by a single site, and singlets cannot form within a single site due to the strong Coulomb repulsion. Thus, the decorated lattice structure is directly responsible for allowing odd-parity singlet superconductors. Similarly, the s^* state sketched in Fig. 1(f) does not have a natural analog on the honeycomb lattice as the triangles are replaced by a single site. Clearly, similar superconducting states should be possible on other decorated lattices. We stress that the f-wave singlet is not an artifact of the 2D model and that this construction works equally well for 3D decorated lattices.

When hole doped, the model displays unconventional superconductivity, Fig. 2. Below the mean-field temperature T_{RVB}, unconventional Cooper pairing is stabilized by the spin exchange interactions.

Superconductivity occurs when the preformed Cooper pairs Bose condense, i.e., when $T < T_{RVB}$ and $T < T_{BEC}$. In quasi-two-dimensional systems [47] $T_{BEC} \approx \frac{1}{2+\ln(\frac{4\gamma}{\pi})}\frac{\delta}{\rho^*} \simeq 1.04\delta$ for the condensation of bosons at the bottom of the lowest DHL band (where $\rho^* = 0.14$ is the density of states, and $\gamma = 100$ quantifies the large anisotropy of the dispersion perpendicular to the lattice plane [47]). We find that $T_c = T_{BEC} = T_{RVB} \approx 0.075t$ at $\delta_c \approx 0.075$ (optimal doping) for $t'/t = J'/J = 1$. The superconducting critical temperature $T_c = T_{BEC}$ for $\delta \leqslant \delta_c$, whereas for $T_c = T_{RVB}$ for $\delta \geqslant \delta_c$. In comparison, for the optimally doped t-J model on the triangular lattice $T_c \sim 0.017t$ [48], suggesting that the flat band in the DHL significantly enhances T_c.

Below $T \approx 0.16t$ we find an RVB state with s^* symmetry for the undoped DHL; this is consistent with exact diagonalization [13,49] on small clusters. Thus we find that s^*

superconductivity emerges at small hole doping in the DHL from a parent insulating state with s^* character. This is highly analogous to the way $d_{x^2-y^2}$ superconductivity arises from hole doping a parent state with $d_{x^2-y^2}$ character in the t-J model on the square lattice [41].

On further doping of the system at $T \to 0$ the pairing symmetry changes at a series of first order superconductor-superconductor transitions. For $0.023 \lesssim \delta \lesssim 0.06$ f-wave pairing occurs; d^* pairing is stabilized in the range $0.1 < \delta < 0.2$; and for other δ, s^* pairing is again present. Above $\delta > 0.22$ the metallic state is recovered. Our numerical analysis finds degenerate d^*_{xy} and $d^*_{x^2-y^2}$ solutions (with the same *free* energy). This contrasts with the $d_{x^2-y^2} + id_{xy}$ solution found in honeycomb [53] and triangular lattices [47,54,55]. We note that these two different types of $d^{(*)}$ solutions [degenerate and $d^{(*)} + id^{(*)}$] are both expected from the symmetry of the (decorated) honeycomb lattice: the Ginzburg-Landau theory of the $d^{(*)}$-order parameters belonging to the E_2 2D irreducible representation, Table I, predicts a $d^{(*)}_{x^2-y^2} + id^{(*)}_{xy}$ state in the weak coupling limit but can also give degenerate $d^{(*)}_{xy}/d^{(*)}_{x^2-y^2}$ states away from the BCS limit [56].

The metallic phases also have unconventional properties [40,46,47,57]. For instance, a pseudogap phase with a spin gap (but no charge gap) emerges for $\delta < \delta_c$ and $T_{BEC} < T < T_{RVB}$. In this phase one expects a dip in the density of states at the Fermi level, in contrast to the peak observed in conventional Fermi liquids. In the present flat band system, our analysis shows that the pseudogap phase is stable to much higher temperatures than in other lattices without flat bands. For $J = 0.1t$ and $\delta \to 0$, we find that the pseudogap temperature $T^* = T_{RVB} \sim 2J$. In contrast $T^* \sim 0.75J$ on the square lattice [46] and $T^* \sim 0.2J$ on the triangular lattice [47,48]. A strange metallic phase is expected to occur in the intermediate doping range for $T > T_{RVB}$ and T_{BEC}, with a Fermi liquid predicted for $T_{BEC} > T > T_{RVB}$ [41].

Anisotropic interactions lead to dramatic changes in the symmetry of the Cooper pairing. Low temperature phase diagrams as a function of doping for different $J'/J = (t'/t)^2$ are shown in Fig. 3. Small J'/J increases the range of dopings in which the f-wave singlet phase is stable but suppresses d^* pairing dramatically. In contrast, at large J'/J, the f-wave solution is no longer realized and s^* pairing dominates the phase diagram. However, at very low doping the s^* and d^* solutions become quasidegenerate, i.e., so close in free energy that we cannot reliably determine which is the lowest energy solution. Thus, while f-wave singlet pairing is more likely to occur at low hole doping and $J'/J \lesssim 1$, d^* pairing would typically arise at larger hole doping.

Raising the temperature also favors s^* pairing. For example we compare the free energies of the lowest energy superconducting solutions to the metallic state for $\delta = 0.15$ in Fig. 4. At low temperatures, d^* pairing occurs over a broad range of exchange anisotropy, $0.5 < J'/J < 1.2$. The d^*-wave solution is much more rapidly suppressed by thermal fluctuations than s^* pairing. Thus at these larger δ we expect an s^* superconductor immediately below T_c, followed by a transition to a d^* state at lower T, cf. Fig. 2.

Significant insight into the temperature and doping variations of the pairing symmetry can be gained from analyzing
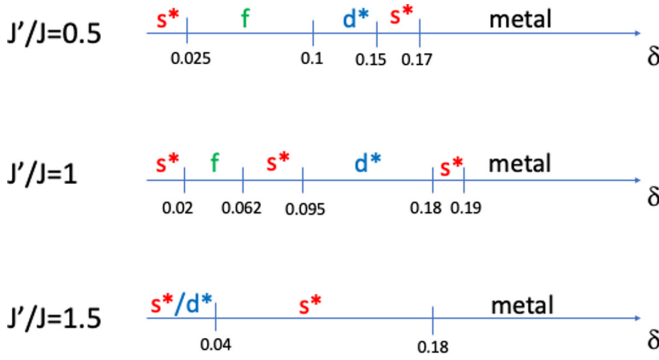
FIG. 3. Dependence of pairing states on exchange anisotropy. For $J' < J$ the f-wave phase is enlarged (relative to $J' = J$) and the d^*-wave phase is reduced. For $J' > J$ the s^* phase dominates with the d^*-wave state only energetically competitive for small doping and the f-wave phase absent. The approximate critical dopings δ for the various transitions are displayed. We have fixed $J/t = 0.1$, $T/t = 0.01$.

a phenomenological weak coupling t-t'-J-J' model where doubly occupied sites are not projected out [49]. The linearized gap equations predict nine possible superconducting states: $s^{(*)}$, f, p_x, p_y, $d_{x^2-y^2}^{(*)}$, and $d_{xy}^{(*)}$ all contained in Table I as expected. In general, the different solutions have different T_c's. The complicated dependence of the T_c's on the coupling, g, indicates that transitions between different superconducting states occur on increasing g (Fig. S5 [49]). The GWA projection effectively amounts to renormalizing the parameters of the t-t'-J-J' model: $(J/t, J'/t) \rightarrow (\tilde{J}/\tilde{t}, \tilde{J}'/\tilde{t}) = \frac{2}{\delta(1+\delta)}(J/t, J'/t)$. Since the effective coupling, $g = \tilde{J}/\tilde{t}$, increases as $\delta \rightarrow 0$, different superconducting states can, in principle, be stabilized in the fully projected model.

The weak coupling t-t'-J-J' model considered allows us to make contact with previous work on superconductivity in
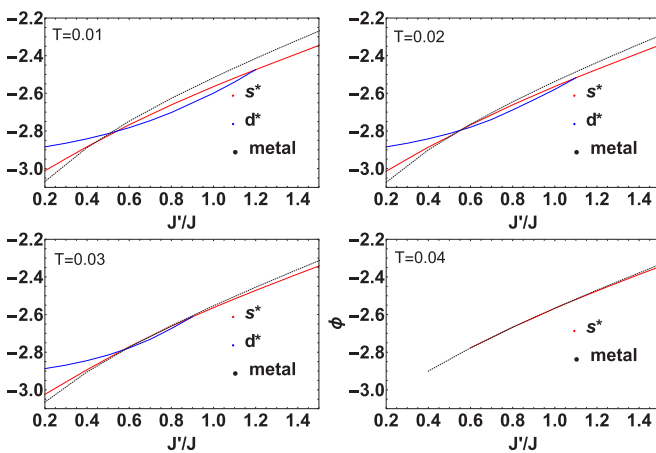

FIG. 4. Dependence of superconducting and metallic free energies on $J'/J = (t'/t)^2$ at fixed doping, $\delta = 0.15$ and $J/t = 0.1$. The free energies at different temperatures of the s^* and d^* pairing states are compared to the metallic solution. Depending on J'/J either s^* or d^* pairing occurs at low temperatures. For $T \gtrsim 0.04t$, superconductivity disappears giving way to a metal for almost any J'/J.

graphene by taking the limit of t'/t, $(J'/J) \rightarrow 0$. In this limit, the DHL band structure is equivalent to two copies of the honeycomb lattice plus two flat bands with a large separation between the molecular orbitals of the triangles [58]. Previous work on an unprojected t-J model on the honeycomb lattice finds d-wave superconductivity [53]. In contrast, in the above limit of our fully projected t-t'-J-J' model, we find quasidegenerate s^* and f-wave superconductivity with a transition to a metallic state occurring at a rather small hole doping, $\delta_c \sim$ 0.045 for $J'/J = 0.1$ ($t'/t \sim 0.326$). Apart from the fact that there are no analogues of the s^* and f-wave states considered here (Fig. 1) on the honeycomb lattice, our analysis on the unprojected t-t'-J-J' model for, say, $J'/J = 0.1$, shows that d^* pairing is the most favorable solution at weak coupling (Fig. S5 [49]) in agreement with [53]. Since the effective couplings $\tilde{J}/\tilde{t}$, $\tilde{J}'/\tilde{t}'$ in our projected t-t'-J-J' model increase as $\delta \rightarrow 0$ we would have expected that the system goes from d^* pairing at large doping (small effective couplings) to s^*/f pairing at small doping. However, our numerical calculations in the projected t-t'-J-J' model show that, as doping is increased, the metallic state sets in before the d^* solution is stabilized. This explains why we do not observe d^* superconductivity in our projected t-t'-J-J' model on the DHL when $J'/J \rightarrow 0$.

The onset of superconductivity in a pure 2D model is associated with vortex-type fluctuations driving the Berezinskii-Kosterlitz-Thouless transition [59,60] at T_{BKT}. However, the organometallic materials we are having in mind here consist of layers of DHLs, weakly coupled in the c direction so they can be regarded as quasi-two-dimensional systems. Thus, the BCS type of superconductivity found in the phase diagram of Fig. 2 is relevant to such materials. On the other hand, one would naively expect that electrons in a flat band should not superconduct since the superfluid weight $D_s \propto n/m^*$ (where n is the electron density) goes to zero as the electron effective mass $m^* \rightarrow \infty$. However, it has been recently shown how a geometric or topological contribution to D_s can be large even when the flat band is far from the rest of the bands [61,62].

V. CONCLUSIONS AND OUTLOOK

Thus, we have seen that flat bands in the DHL provide a route to exotic, high-temperature superconductivity. In particular we predict unconventional s^*, d^*, and f-wave singlet superconducting states competing with one another due to the complex structure of the lattice which produces the flat band. The flat band at the Fermi energy enhances both the superconducting critical temperature and the pseudogap temperature scale compared to other lattices studied with comparable theories. To quantify this, let us assume that the doped DHL can be experimentally realized in organic or organometallic materials. This can be achieved by applying external negative pressures on $Mo_3S_7(dmit)_3$ (dmit=1,3-dithiol-2-thione-4,5-dithiolate) suppressing interlayer coupling or, at ambient pressure, in $Rb_{3-\delta}Sr_\delta TT \cdot 2H_2O$ whose weakly coupled DHLs of TT molecules alternate with Rb layers. For $Mo_3S_7(dmit)_3$ (dmit=1,3-dithiol-2-thione-4,5-dithiolate) $t' \approx t = 0.05$ eV [58], taking $J' = J = 0.1t$ yields $T_c \sim 44$ K at optimal doping. In the half-filled insulating material $Rb_3TT \cdot 2H_2O$ (TT=triptycene tribenzoquinone) the largest hopping integral is an order of magnitude greater than

the largest hopping integral in $Mo_3S_7(dmit)_3$ [21], suggesting, surprisingly, that superconductivity may survive to even higher temperatures of the order of ~10^2 K. In $Rb_3TT \cdot 2H_2O$ the t and t' are negative so the flat band lies below the Fermi energy and electron (rather than hole) doping promises flat band superconductivity; this might be achieved via the synthesis of $Rb_{3-\delta}Sr_\delta TT \cdot 2H_2O$.

[1] Y. Cao, V. Fatemi, S. Fang, K. Watanabe, T. Taniguchi, E. Kaxiras, and P. Jarillo-Herrero, Nature (London) **556**, 43 (2018).

[2] Y. Cao, V. Fatemi, A. Demir, S. Fang, S. L. Tomarken, J. Y. Luo, J. D. Sanchez-Yamagishi, K. Watanabe, T. Taniguchi, E. Kaxiras, R. C. Ashoori, and P. Jarillo-Herrero, Nature (London) **556**, 80 (2018).

[3] L. Balents, C. R. Dean, D. K. Efetov, and A. F. Young, Nat. Phys. **16**, 725 (2020).

[4] S. Sayyad, E. W. Huang, M. Kitatani, M.-S. Vaezi, Z. Nussinov, A. Vaezi, and H. Aoki, Phys. Rev. B **101**, 014501 (2020).

[5] G. E. Volovik, JETP Lett. **107**, 516 (2018).

[6] T. T. Heikkilä, N. B. Kopnin, and G. E. Volovik, JETP Lett. **94**, 233 (2011).

[7] N. B. Kopnin, T. T. Heikkilä, and G. E. Volovik, Phys. Rev. B **83**, 220503(R) (2011).

[8] H. Aoki, J. Supercond. Nov. Magn. **33**, 2341 (2020).

[9] A. Rüegg, J. Wen, and G. A. Fiete, Phys. Rev. B **81**, 205115 (2010).

[10] J. Wen, A. Rüegg, C.-C. Joseph Wang, and G. A. Fiete, Phys. Rev. B **82**, 075125 (2010).

[11] M. Chen, H.-Y. Hui, S. Tewari, and V. W. Scarola, Phys. Rev. B **97**, 035114 (2018).

[12] M. F. López and J. Merino, Phys. Rev. B **100**, 075154 (2019).

[13] M. F. López and J. Merino, Phys. Rev. B **102**, 035157 (2020).

[14] D.-S. Ma, Y. Xu, C. S. Chiu, N. Regnault, A. A. Houck, Z. Song, and B. A. Bernevig, Phys. Rev. Lett. **125**, 266403 (2020).

[15] H. L. Nourse, R. H. McKenzie, and B. J. Powell, Phys. Rev. B **103**, L081114 (2021).

[16] A. L. Khosla, A. C. Jacko, J. Merino, and B. J. Powell, Phys. Rev. B **95**, 115109 (2017).

[17] A. C. Jacko, A. L. Khosla, J. Merino, and B. J. Powell, Phys. Rev. B **95**, 155120 (2017).

[18] J. Merino, A. C. Jacko, A. L. Khosla, and B. J. Powell, Phys. Rev. B **96**, 205118 (2017).

[19] B. J. Powell, J. Merino, A. L. Khosla, and A. C. Jacko, Phys. Rev. B **95**, 094432 (2017).

[20] R. Llusar, S. Uriel, C. Vicent, J. M. Clemente-Juan, E. Coronado, C. J. Gomez-Garcia, B. Braida, and E. Canadell, J. Am. Chem. Soc. **126**, 12076 (2004).

[21] Y. Shuku, A. Mizuno, R. Ushiroguchi, C. S. Hyun, Y. J. Ryu, B.-K. An, J. E. Kwon, S. Y. Park, M. Tsuchiizu, and K. Awaga, Chem. Commun. **54**, 3815 (2018).

[22] Y.-Z. Zheng, M.-L. Tong, W. Xue, W.-X. Zhang, X.-M. Chen, F. Grandjean, and G. J. Long, Angew. Chem. Int. Ed. **46**, 6076 (2007).

[23] K. M. Henline, C. Wang, R. D. Pike, J. C. Ahern, B. Sousa, H. H. Patterson, A. T. Kerr, and C. L. Cahill, Cryst. Growth Des. **14**, 1449 (2014).

[24] L. M. Henling and R. E. Marsh, Acta Crystallogr., Sect. C **70**, 834 (2014), CSD-FAZGIY.

[25] H.-F. Lin, Y.-H. Chen, H.-D. Liu, H.-S. Tao, and W.-M. Liu, Phys. Rev. A **90**, 053627 (2014).

[26] R. Nandkishore, R. Thomale, and A. V. Chubukov, Phys. Rev. B **89**, 144501 (2014).

[27] H. Guo, X. Zhu, S. Feng, and R. T. Scalettar, Phys. Rev. B **97**, 235453 (2018).

[28] R. Gholami, R. Moradian, S. Moradian, and W. E. Pickett, Sci. Rep. **8**, 13795 (2018).

[29] J. Richter, J. Schulenburg, A. Honecker, and D. Schmalfuss, Phys. Rev. B **70**, 174454 (2004).

[30] S. S. Jahromi and R. Orús, Phys. Rev. B **98**, 155108 (2018).

[31] H. Yao and S. A. Kivelson, Phys. Rev. Lett. **99**, 247203 (2007).

[32] V. Elser, Phys. Rev. Lett. **62**, 2405 (1989).

[33] P. Lecheminant, B. Bernu, C. Lhuillier, L. Pierre, and P. Sindzingre, Phys. Rev. B **56**, 2521 (1997).

[34] R. R. P. Singh and D. A. Huse, Phys. Rev. B **76**, 180407(R) (2007).

[35] S. Yan, D. A. Huse, and S. R. White, Science **332**, 1173 (2011).

[36] O. I. Motrunich, Phys. Rev. B **72**, 045105 (2005).

[37] M. Holt, B. J. Powell, and J. Merino, Phys. Rev. B **89**, 174415 (2014).

[38] J. Merino, M. Holt, and B. J. Powell, Phys. Rev. B **89**, 245112 (2014).

[39] E. P. Kenny, G. David, N. Ferré, A. C. Jacko, and B. J. Powell, Phys. Rev. Materials **4**, 044403 (2020).

[40] P. W. Anderson, Science **235**, 4793 (1987).

[41] P. A. Lee, N. Nagaosa, and X.-G. Wen, Rev. Mod. Phys. **78**, 17 (2006).

[42] B. J. Powell and R. H. McKenzie, Phys. Rev. Lett. **98**, 027005 (2007).

[43] B. J. Powell and R. H. McKenzie, Phys. Rev. Lett. **94**, 047004 (2005).

[44] D. J. Scalapino, Rev. Mod. Phys. **84**, 1383 (2012).

[45] E. M. Nica and Q. Si, npj Quant. Mat. **6**, 3 (2021).

[46] G. Kotliar and J. Liu, Phys. Rev. B **38**, 5142 (1988).

[47] B. Kumar and B. S. Shastry, Phys. Rev. B **68**, 104508 (2003); **69**, 059901(E) (2004).

[48] Q. H. Wang, D. H. Lee, and P. A. Lee, Phys. Rev. B **69**, 092504 (2004).

[49] See Supplemental Material at http://link.aps.org/supplemental/10.1103/PhysRevB.103.094517 for full details of the RVB calculations.

[50] G. Baskaran, Phys. Rev. B **65**, 212505 (2002).

[51] J. Merino and O. Gunnarsson, Phys. Rev. B **89**, 245130 (2014).

[52] A $f_{y(3x^2-y^2)}$ state constructed from singlets along the t' bonds (with nodes along the t bonds) is also possible but would treble the size of the unit cell.

[53] A. M. Black-Schaffer and S. Doniach, Phys. Rev. B **75**, 134512 (2007).

[54] G. Baskaran, Phys. Rev. Lett. **91**, 097003 (2003).

[55] M. Ogata, J. Phys. Soc. Jpn. **72**, 1839 (2003).

[56] B. J. Powell, J. Phys. Cond. Matt. **18**, L575 (2006).

[57] G. Baskaran, Z. Zou, and P. W. Anderson, Solid State Commun. **63**, 973 (1987).

[58] A. C. Jacko, C. Janani, K. Koepernik, and B. J. Powell, Phys. Rev. B **91**, 125140 (2015).

[59] V. L. Berezinskii, Zh. Eksp. Teor. Fiz. **59**, 907 (1971) [Sov. Phys. JETP **32**, 493 (1971)].

[60] J. M. Kosterlitz and D. J. Thouless, J. Phys. C **6**, 1181 (1973).

[61] X. Hu, T. Hyart, D. I. Pikulin, and E. Rossi, Phys. Rev. Lett. **123**, 237002 (2019).

[62] F. Xie, Z. Song, B. Lian, and B. A. Bernevig, Phys. Rev. Lett. **124**, 167002 (2020).